IEEE Access
Multidisciplinary | Rapid Review | Open Access Journal

Received January 18, 2021, accepted January 21, 2021, date of publication February 1, 2021, date of current version February 9, 2021.

Digital Object Identifier 10.1109/ACCESS.2021.3056226

Wind Generator Impedance Matching in Small-Scale Passive Wind Energy Systems

CASPER J. J. LABUSCHAGNE, (Student Member, IEEE), AND MAARTEN J. KAMPER, (Senior Member, IEEE)
Department of Electrical and Electronic Engineering, Stellenbosch University, Stellenbosch 7600, South Africa

Corresponding author: Casper J. J. Labuschagne (17539455@sun.ac.za)

This work was supported in part by the Centre for Renewable and Sustainable Energy Studies at Stellenbosch University, Stellenbosch, South Africa, and in part by the Department of Science and Technology of South Africa.

ABSTRACT In this paper, the improved turbine power matching of passive wind energy systems for dc-connected battery storage applications with an impedance matching method is investigated. The passive system uses a direct-drive permanent magnet synchronous generator and is directly connected via a diode rectifier to the dc fixed-voltage battery storage. To improve power matching, an external inductance is added to the passive system between the generator and the diode rectifier. A static finite element based solution method is proposed to accurately calculate the necessary external inductance to achieve near maximum power point matching. It is shown that the proposed finite element based calculation method is computationally efficient and excellently suited for generator design optimization, which is critical for this application. It is also shown that by rewinding existing machines for the correct cut-in speed and adding the external inductance for improved power matching, existing machines can be effectively recycled for passive wind energy systems. The proposed static finite element solution method's accuracy and improved power matching are confirmed with measured results on a sub 5 kW power level.

INDEX TERMS Impedance matching, passive wind energy system, permanent magnet synchronous generator, power matching, small-scale wind turbine, wind energy.

I. NOMENCLATURE

α, δ	Current/load angle (°)
η	Generator efficiency
λ_{uv}	Slot permeance factor
λ_{PM}	PM flux linkage (Wb)
ω_m	Mechanical turbine speed (rad/s)
ω_s	Synchronous electrical speed (rad/s)
τ_d	Differential harmonic leakage flux coefficient
B_t, B_{yh}	Maximum stator tooth/yoke flux density (T)
c, x, y	Steinmetz coefficients
d_i, d_o	Airgap/outer diameter (mm)
d, q	Subscripts denoting direct- and quadrature axis values
E_g	Induced generator voltage (V)
f_s	Synchronous electrical frequency (Hz)
g_{air}	Mechanical air gap (mm)
I_s	Generator current (A)
I_{rms}	RMS current (A)
J	Generator current density (A/mm^2)
k_w	Winding factor
K_s	Saturation factor
l	Axial length (mm)
L_c	Transmission cable inductance (mH)
L_e, L_i, L_s	End-winding/internal/synchronous inductance (mH)
L_m, L_{sl}	Magnetization/slot-leakage inductance (mH)
L_{ext}, $L_{1,2,3}$	External inductance (mH)
m	Number of phases
M_{active}, M_{PM}	Generator's active/PM mass (kg)
M_t, M_{yh}	Stator tooth/yoke mass (kg)
n_c, n_r	Cut-in/rated turbine speed (r/min)
N_s	Number of turns per coil
p	Number of poles
P_{cu}, P_{core}	Generator copper/core losses (kW)
P_g	Generated power (kW)
P_t	Turbine power (kW)
Q_s	Number of stator slots

The associate editor coordinating the review of this manuscript and approving it for publication was Ton Duc Do.

R_{ac}	Internal battery storage resistance referred to ac-side of diode rectifier (Ω)
R_{bat}	Internal battery storage resistance (Ω)
R_c	Combined resistance of brush-slip-rings and transmission cable (Ω)
R_e, R_i, R_s	End-winding/internal/synchronous resistance (Ω)
R_{ext}	External inductor's resistance (Ω)
R_{st}	Equivalent per phase resistance (Ω)
T_g	Generated torque (Nm)
V_{bat}	Battery storage terminal voltage (V)
V_b	Battery storage terminal voltage referred to ac-side of diode rectifier (V)
V_{diode}	Forward diode voltage drop (V)
V_{rms}	RMS voltage (V)
W	Number of turns in series per phase
X_e	End-winding reactance (Ω)
X_{ext}	External reactance (Ω)
Z_c	Combined impedance of brush-slip-rings and transmission cable (Ω)
Z_s	Synchronous impedance (Ω)
Z_{ext}	External impedance (Ω)

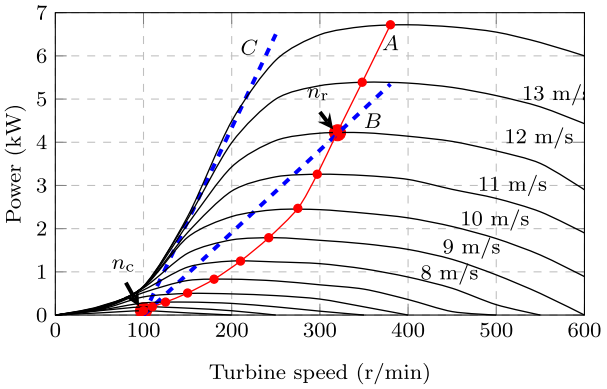

FIGURE 1. Wind turbine power versus turbine speed curves with wind speed a parameter, with examples of actively controlled (curve *A*) and passive uncontrolled (curves *B* and *C*) operating power curves.

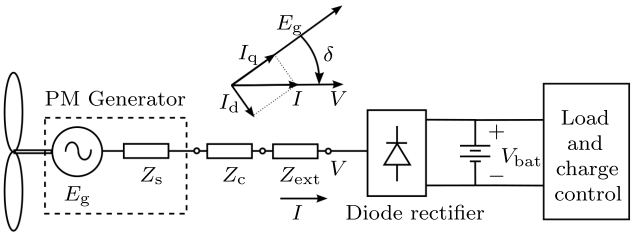

FIGURE 2. Single line diagram of PM wind generator connected to passive system with uncontrolled diode rectifier and battery storage.

II. INTRODUCTION

Wind and hybrid photovoltaic (PV) energy systems with battery storage are attractive options for ac- or dc microgrids in remote communities where utility grid connection is too expensive. With the relatively cheap PV systems available nowadays, there is a lot of pressure to make small-scale (< 20 kW) wind energy conversion systems (WECS) much cheaper. This incentivizes the need to reduce cost, which directly affects the reliability and the control of the generators and the power converters that operate between the turbine and the battery storage.

Considering small-scale WECSs, there is always the aim to operate the system at maximum power point in order to maximize energy harvesting. The power versus speed curves of a small-scale wind turbine are shown in Fig. 1, with the maximum power points of the turbine indicated by power curve *A*. Maximum power point tracking (MPPT) of the system can be obtained by using power electronic converters, such as active synchronous rectifiers or dc-to-dc converters, along with rather complex MPPT algorithms [1]–[3]. However, according to [4], the most common cause of failure in stand-alone WECSs is the failure of the power electronic converters. Therefore, consider the simple passive WECS in Fig. 2. Neither an active synchronous rectifier nor a dc-to-dc converter is used; instead, the generator is connected directly to the battery storage via a passive diode bridge rectifier. This minimizes power electronics in the system, thereby reducing the cost and increasing the reliability of the system [5], [6]. Thus making the passive WECS in Fig. 2 an attractive option for developing countries, especially in Africa, and for industry.

From a generator perspective, for a small-scale WECS, the permanent magnet synchronous generator (PMSG) and the squirrel cage induction generator are identified by [7] as distinctively suitable generators. However, despite the volatile cost of PM material, the use of PMSGs in small-scale wind generator applications is far more popular in industry [8]. Low cogging torque is essential for this application. Therefore, integral-slot windings are not ideal and it is standard to use fractional-slot overlapping or non-overlapping windings for the PMSGs.

Power curve *B* in Fig. 1 shows the desired power matching for the passive system where the wind generator cuts in at the specified speed, n_c, and matches the maximum power of the wind turbine at the rated wind and turbine speed indicated by n_r. Because the passive system uses no method of control, the PMSG's internal impedance, Z_s, in Fig. 2 needs to match correctly with the load voltage to ensure that the wind generator's power matches with the available power from the wind turbine at the maximum power point. Designing the PMSG for this natural impedance matching, so that better power matching is achieved at all wind speeds, is difficult (power curve *C* resembles that of a typical PMSG). In [9], the PMSG is designed and then the wind turbine's parameters are adjusted for better impedance matching. However, changing the wind turbine's parameters is not always desirable. In [6], [10] and [11], the PMSGs are designed by optimizing impedance matching for a perceived "typical wind cycle". This design approach neglects to design for a specified cut-in speed for the wind generator and therefore

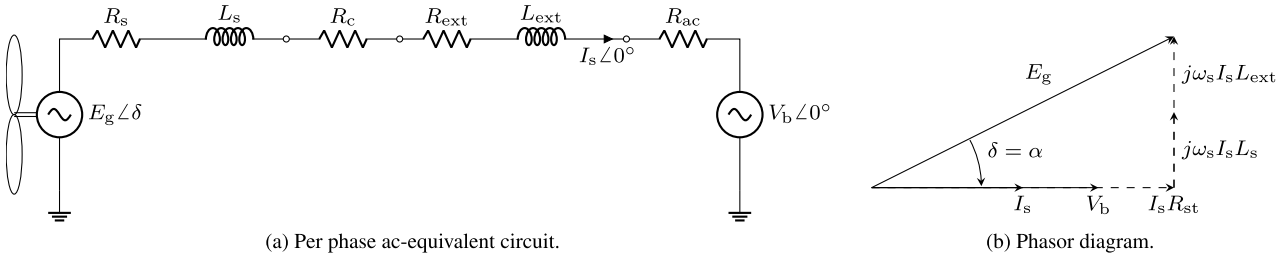

(a) Per phase ac-equivalent circuit.

(b) Phasor diagram.

FIGURE 3. Analytical modelling of the passive wind generator system.

does not necessarily guarantee good power matching at low wind speeds. This is particularly important for small-scale WECSs, as these systems are more often deployed according to need as opposed to being deployed at the optimal wind site. Small-scale WECSs therefore mostly operate under low wind speed conditions and it is highlighted by [12] how important it is for manufacturers to take this into account.

In [13] and [14] an impedance matching method is used whereby an external inductance is added between the generator and the diode bridge rectifier, as shown in Fig. 2 (Z_{ext}). This method of impedance matching ensures good power matching between the generator and the wind turbine and resembles power curve *B* in Fig. 1. With the correct inductance added for external impedance matching, effectively any generator can be matched with any wind turbine, provided that the generator's rated power is sufficient. This also complements research on recycling electrical machines for small-scale WECSs [15], [16]. Another additional advantage of the externally connected inductance is that it inadvertently addresses the issue of discontinuous current due to commutation [17] and ensures sinusoidal generator line currents flowing into the diode rectifier [18]. This improves the torque quality and reduces the noise of the PMSG [19].

In [13], the impedance matching with an external inductance was for a passive WECS with an *air-cored* PMSG. However, when using an *iron-cored* PMSG, the necessary external inductance calculation is much more challenging. With iron-cored PMSGs the effect of saturation and armature reaction must be taken into account very accurately. More so in this case, with the relatively large demagnetization *d*-axis current in the generator, as shown in Fig. 2. In [14], an iron-cored PMSG was investigated for a passive WECS. However, it is found that the method therein to calculate the external inductance is prone to inaccuracies and impractical in the PMSG design process. The calculation method presented in [14] is thus deemed insufficient. Hence, in this paper an accurate and computer efficient static finite element analysis (FEA) solution method is proposed to calculate the necessary external inductance, that improves on the calculation methods in [13] and [14].

The aim of this paper is to investigate and to demonstrate the extent to which impedance matching can be applied in passive WECSs to improve power matching. Subsequently, a necessary and accurate solution method to calculate the external inductance for impedance matching is also presented.

The paper layout is as follows: Section III gives an overview of the analytical modelling and calculations to determine the external inductance for impedance matching. Section IV describes the equivalent modelling for the proposed solution method. Section V then discusses the proposed solution method to more accurately calculate the necessary external inductance. Design results and case studies are presented in Sections VI to VIII. The results are verified with practical measurements in Section IX.

III. IMPEDANCE MATCHING WITH ANALYTICAL METHOD

In this section, an analytical calculation for the external inductance, L_{ext}, in Fig. 2 is given. This analytical calculation is used as an initial estimation for the solution method described in Section V. The per phase ac-equivalent circuit of the passive WECS in Fig. 2 is given in Fig. 3(a). The resulting phasor diagram in Fig. 3(b) is used for the analytical calculation.

A. BATTERY STORAGE

For the passive WECS's analysis, the battery storage in Fig. 2 is typically modelled as a dc voltage, V_{bat}, in series with an internal resistance, R_{bat} [13]. The dc voltage, V_{bat}, and the forward voltage drop across a diode in the diode rectifier, V_{diode}, are used to calculate the fundamental phase voltage on the ac side of the diode rectifier as

$$V_b = \frac{\sqrt{2}(V_{bat} + 2V_{diode})}{\pi}, \tag{1}$$

and is shown in Fig. 3(a). The internal battery resistance is also referred to the ac side of the diode bridge rectifier as an ac-equivalent resistance, using

$$R_{ac} = \frac{6R_{bat}}{\pi^2}. \tag{2}$$

B. SYSTEM IMPEDANCE

The per phase synchronous inductance of the PMSG in Fig. 3 is calculated as

$$\begin{aligned} L_s &= L_i + L_e \\ &= L_m(1 + \tau_d) + L_{sl} + L_e, \end{aligned} \tag{3}$$

with the analytical formulae for the magnetization inductance L_m, the differential harmonic leakage flux coefficient τ_d, and the slot-leakage inductance L_{sl} given in Appendix A. The per phase end-winding inductance, L_e, can be calculated using the analytical approximations in [20] for non-overlapping winding PM machines, or with that of [21] in the case of PM machines with overlapping windings. The WECS's cable inductance, L_c, is considered negligible in the analysis, but can be incorporated if significant.

R_{st} in Fig. 3(b) is the equivalent per phase resistance given by

$$\begin{aligned} R_{st} &= R_s + R_c + R_{ext} + R_{ac} \\ &= R_i + R_e + R_c + R_{ext} + R_{ac}. \end{aligned} \tag{4}$$

In (4), R_i is the internal generator resistance, R_e the generator end-winding resistance, R_c the resistance of the brush-slip-rings in the nacelle and transmission cable (more information on the wind turbine is given in Appendix B), and R_{ext} is the resistance of the external inductance.

C. EXTERNAL INDUCTANCE CALCULATION

The passive WECS, with an uncontrolled diode bridge rectifier and a fixed voltage on the dc side will operate at a unity displacement power factor [17]. As shown in Fig. 3, the generator current, I_s, is in phase with the fundamental component of the terminal voltage, V_b, at the diode rectifier. Hence the current angle, α, is equal to the load angle, δ, between the induced generator voltage E_g and the terminal voltage V_b, shown in Fig. 3(b).

The induced generator voltage at the rated operating point can be calculated using the relationship between E_g and the turbine speed, as given in (5). Since V_b is equal to the induced generator voltage at cut-in speed n_c, the induced generator voltage at rated speed n_r is given by

$$E_{g(r)} = V_b \frac{n_r}{n_c}. \tag{5}$$

As it is a small-scale WECS, the core and wind-and-friction losses of the generator are further ignored. Thus, the generated power, P_g, is assumed equal to the known turbine power, P_t:

$$P_g = 3E_{g(r)} I_s \cos\delta \approx P_t. \tag{6}$$

From Fig. 3(b), $\cos\delta$ is calculated as

$$\cos\delta = \frac{V_b + I_s R_{st}}{E_{g(r)}}. \tag{7}$$

By substituting (7) into (6) and solving the quadratic equation, the rated current is given by

$$I_s = \frac{\sqrt{V_b^2 + \frac{4}{3} R_{st} P_g} - V_b}{2R_{st}}. \tag{8}$$

With I_s known, the load angle δ can now be calculated from (7). Also from Fig. 3(b),

$$\sin\delta = \frac{I_s \omega_s (L_s + L_{ext})}{E_{g(r)}}. \tag{9}$$

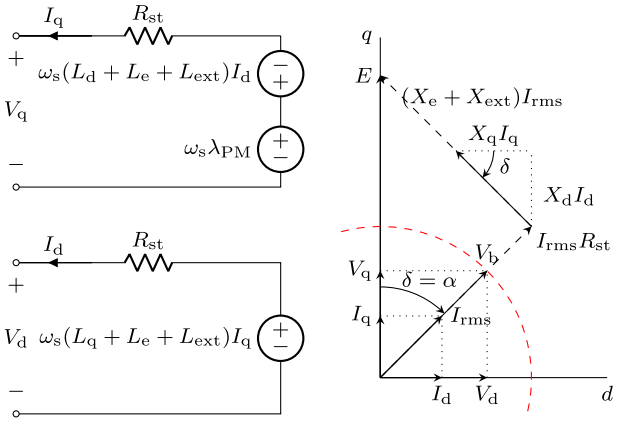

(a) Per phase dq-equivalent circuit diagram. (b) Vector diagram.

FIGURE 4. Equivalent *dq*-modelling.

Subsequently, L_{ext} is calculated analytically by rewriting (9) as

$$L_{ext} = \left(\frac{60V_b}{\pi p n_c}\right)\frac{\sin\delta}{I_s} - L_s, \tag{10}$$

where p is the number of poles and L_s is calculated analytically from (3).

IV. EQUIVALENT PASSIVE WECS MODELLING

In the previous section, an approximated per phase model is used to analytically estimate L_{ext}. However, a more detailed model of the machine is necessary for an accurate calculation of L_{ext}. In this section, the equivalent modelling used for the proposed solution method in Section V is discussed.

A. EQUIVALENT CIRCUIT dq-MODELLING

The PMSG modelling for the static FEA is done in the steady-state and with the dq-reference frame fixed to the PM rotor. Fig. 4 shows the dq-equivalent circuits and the resulting vector diagram for the passive WECS in Fig. 2.

The steady-state dq-equations can be derived from the dq-equivalent circuits in Fig. 4(a), as

$$V_q = -R_{st} I_q - \omega_s (L_d + L_e + L_{ext}) I_d + \omega_s \lambda_{PM} \tag{11}$$

$$V_d = -R_{st} I_d + \omega_s (L_q + L_e + L_{ext}) I_q, \tag{12}$$

where ω_s is the synchronous electrical speed and R_{st} is the same as in (4). The dq-inductances, L_q and L_d, are given by (13) and (14) respectively.

$$L_q = \frac{\lambda_q}{-I_q} \tag{13}$$

$$L_d = \frac{\lambda_d - \lambda_{PM}}{-I_d} \tag{14}$$

The general relations of voltage and current are given by

$$\begin{bmatrix} V_q \\ V_d \end{bmatrix} = \sqrt{2} V_{rms} \begin{bmatrix} \cos\delta \\ \sin\delta \end{bmatrix}$$

$$\begin{bmatrix} I_q \\ I_d \end{bmatrix} = \sqrt{2} I_{rms} \begin{bmatrix} \cos\alpha \\ \sin\alpha \end{bmatrix}, \tag{15}$$

where V_{rms} is the RMS value of the fixed voltage on the ac side of the uncontrolled diode rectifier, i.e. $V_{rms} = V_b$ of (1).

B. PERFORMANCE

The developed torque and the electrical power generated by the PMSG are calculated using (16) and (17) respectively.

$$T_g = \frac{3}{4}p[(L_q - L_d)I_dI_q + \lambda_{PM}I_q] \tag{16}$$

$$P_g = T_g\omega_m \tag{17}$$

The efficiency of the PMSG is calculated using

$$\eta = \frac{P_g - P_{cu}}{P_g + P_{core}}, \tag{18}$$

where P_{cu} is the copper losses and P_{core} is the iron core losses in the stator. To simplify the efficiency calculation, wind- and friction losses are ignored. Copper losses are calculated as

$$P_{cu} = 3{I_{rms}}^2R_s. \tag{19}$$

The core losses are calculated by a semi-analytical method, expressed as

$$P_{core} = cf_s^{\,x}({B_t}^yM_t + {B_{yh}}^yM_{yh}), \tag{20}$$

using Steinmetz coefficients and static FEA. B_t and B_{yh} are static FEA calculated maximum flux densities in the teeth and the yoke of the PMSG stator respectively. M_t and M_{yh} are the respective tooth- and yoke iron masses. The calculation is done at the PMSG's electrical frequency f_s, at the rated turbine operating speed n_r. The Steinmetz coefficients c, x and y are predetermined coefficients. (The material used in Section VI is M-19 29 Ga, with the coefficients $c = 0.00968569$, $x = 1.19792$ and $y = 1.79564$.)

V. STATIC FEA SOLUTION METHOD

To calculate the PMSG's performance from the equivalent modelling discussed in the previous section, a solution method is necessary: The PMSG is connected to an uncontrolled passive system and thus the current-loading of the PMSG at a certain speed is unknown. The addition of an unknown external inductance, L_{ext}, for maximum power matching, further complicates the solution method. In order to calculate the machine performance at rated speed, as explained in Section IV, the PMSG's current and load angle are solved iteratively using multiple static FEA solutions, as explained in the following subsections.

A. REWRITING THE STEADY-STATE EQUATIONS

The steady-state dq-equations of the PMSG need to be rewritten in order to solve the unknowns that are necessary to calculate the PMSG performance. Equations (11) and (12) are rewritten by substituting the dq-values for voltage and current with their equivalent RMS values from (15). Then, by rewriting (11) and (12) in terms of I_{rms}, it gives

$$I_{rms} = \frac{\sqrt{2}V_{rms}\cos\delta - \omega_s\lambda_{PM}}{\sqrt{2}(-R_{st}\cos\delta - \omega_s(L_q + L_e + L_{ext})\sin\delta)} \tag{21}$$

and

$$I_{rms} = \frac{\sqrt{2}V_{rms}\sin\delta}{\sqrt{2}(-R_{st}\sin\delta + \omega_s(L_d + L_e + L_{ext})\cos\delta)}. \tag{22}$$

Equations (21) and (22) are used to numerically solve for δ and I_{rms}.

B. EXTERNAL INDUCTANCE CALCULATION

If the value of L_{ext} in (21) and (22) is known, then the PMSG's static FEA solutions can be used to evaluate its performance at the rated speed. By choosing three values for L_{ext} (L_1, L_2, L_3) and calculating the PMSG's performance for these three values, a second degree polynomial of the Newton form

$$f_2(y) = c_1c_2(y - y_1) + c_3(y - y_1)(y - y_2) \tag{23}$$

can be determined in terms of the generated power P_g and L_{ext}. The second degree polynomial of (23) is thus rewritten as

$$P_g(L_{ext}) = c_1c_2(L_{ext} - L_1) + c_3(L_{ext} - L_1)(L_{ext} - L_2). \tag{24}$$

Using the three generated power values $P_g(L_1)$, $P_g(L_2)$, $P_g(L_3)$, and their corresponding external inductance values L_1, L_2, L_3, the coefficients in (24) are calculated as

$$c_1 = P_g(L_1), \quad c_2 = \frac{P_g(L_1) - P_g(L_2)}{L_1 - L_2} \quad \text{and}$$
$$c_3 = \frac{c_2}{L_1 - L_3} - \frac{P_g(L_2) - P_g(L_3)}{(L_2 - L_3)(L_1 - L_3)}. \tag{25}$$

An example of the calculated second degree polynomial is illustrated in Fig. 5(b). L_{ext} is calculated by substituting the rated generator power at rated speed into (24), i.e. $P_g(L_{ext})$. For the solution to be valid, the values for L_1 and L_3 have to bracket the solution value of L_{ext}. To estimate values for L_1, L_2 and L_3, the analytical calculation in (10) is used, whereby it is taken that $L_2 = L_{ext(10)}$ and then choosing values for L_1 and L_3 such that $L_1 < L_{ext(10)} < L_3$.

C. SOLUTION METHOD PROCEDURE

To externally match the impedance of the PMSG with the load in Fig. 2, the solution method in Fig. 6 can be used. This method implements the L_{ext} calculation in Fig. 5 by using static FEA iterations to calculate the PMSG's performance. The following steps are done:

1) The induced generator voltage at cut-in speed n_c needs to be equal to the voltage at the battery terminals, V_b, with zero generator current flowing. The dq-equations (11) and (12) at n_c are thus, $V_q = \omega_s\lambda_{PM}$ and $V_d = 0$. It is thus necessary to alter λ_{PM} by calculating the number of turns per coil N_s that produces the desired value for λ_{PM}. This is done with the first static FEA solution.
2) Estimate L_1, L_2 and L_3 analytically using (10).
3) The external inductance is set equal to the first predetermined value, $L_{ext} = L_1$. For a starting point, the first static FEA iteration is run with δ and I_{rms} set to the analytically calculated values using (7) and (8).
4) Using the results from the previous static FEA iteration, equations (21) and (22) are solved simultaneously to calculate I_{rms} and δ, knowing that $0° \leq \delta \leq 90°$. Two static FEA iterations are now run to determine more

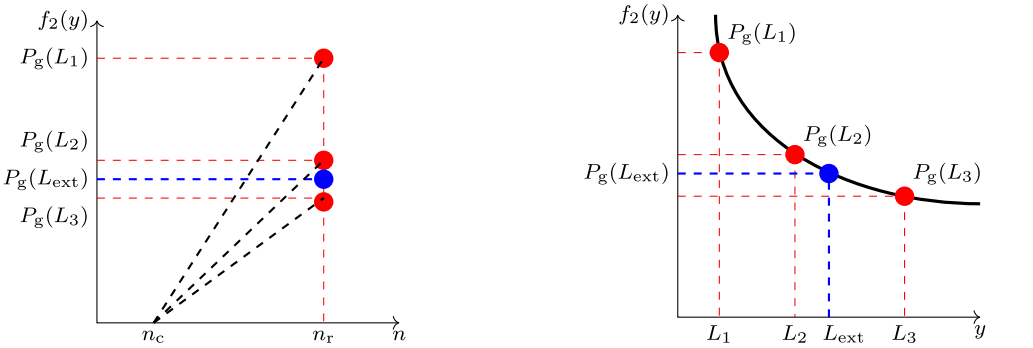

(a) Generated power, calculated at rated speed, with L_1,L_2 and L_3 added to the system. Collectively this brackets $P_g(L_{ext})$ and ensures accuracy.

(b) Second degree polynomial curve fitting through three power points, from which L_{ext} is calculated knowing the rated power $P_g(L_{ext})$.

FIGURE 5. Visual representation of the external inductance calculation.

accurate values for I_{rms} and δ by solving (21) and (22). These two static FEA iterations are deemed acceptable and accurate for current I_{rms} convergence.

5) Step 4 is now repeated for $L_{ext} = L_2$ and $L_{ext} = L_3$ (thus obtaining points $P_g(L_1)$, $P_g(L_2)$ and $P_g(L_3)$ as illustrated in Fig. 5(a)).
6) The calculated performance results are then used to determine the second degree polynomial of (24) and (25). By inspecting the obtained second degree polynomial, the final value for the added external inductance L_{ext} is calculated using the specified rated power (this step is also shown in Fig. 5(b)).
7) The generator's rated current, I_{rms}, and load angle, δ, is once more solved as in step 4. From this final solution, the performance evaluation of the generator is done using equations (16)-(18) to determine if it complies with the design specifications.

VI. STATIC FEA SOLUTION METHOD RESULTS

In this section, two case studies are presented to investigate the application of external impedance matching as a method to improve power matching in passive WECSs. Two direct-drive non-overlapping winding PMSGs (NO-PMSG), G_1 and G_2, are considered. Generator G_1 is for a 4.2 kW passive WECS and G_2 for a 12.5 kW passive WECS. The cross sections of the NO-PMSGs are shown in Fig. 7, with some design detail given in Table 1. The desired operating points for the respective wind turbines are summarised in Table 2.

A. 4.2 kW NO-PMSG IMPEDANCE MATCHING (G_1)

For generator G_1, the outer dimensions in Table 1 are according to the dimensional constraints of the wind turbine (shown in Fig. 14, Appendix B). Other relevant dimensions were determined using initial sizing estimations.

The static FEA solution results for the impedance matching of G_1 are summarized in Table 3. It is shown in Table 3 that, with the calculated L_{ext} added to the passive WECS, G_1 matches with the rated generated power P_g at the specified operating point in Table 2.

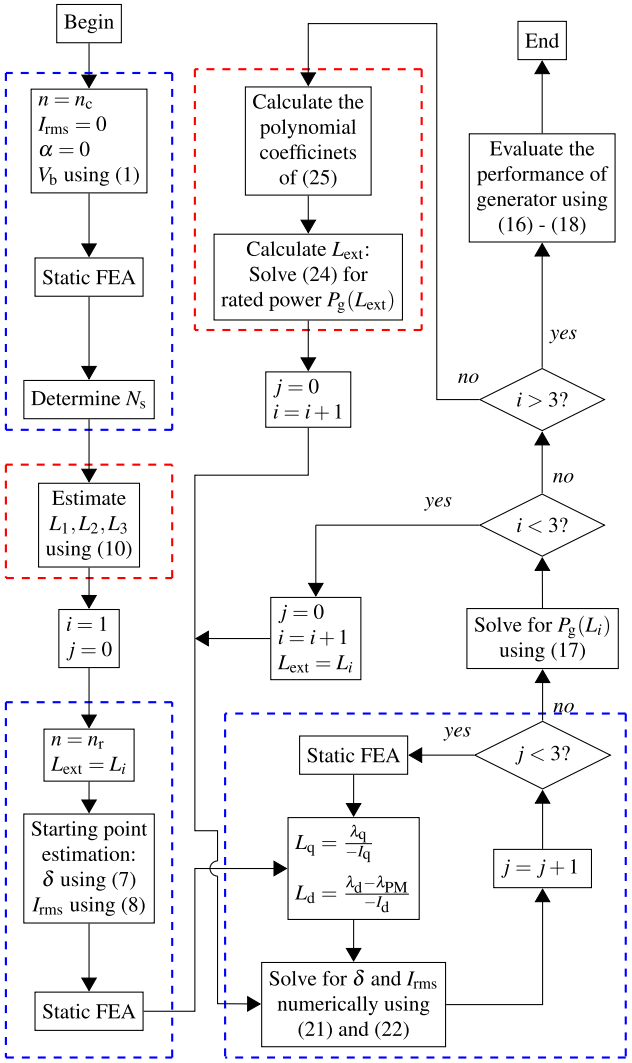

FIGURE 6. Static FEA solution method used to calculate L_{ext} for impedance matching and to evaluate the PMSG's performance. i = changing L_{ext} values [$L_{ext} = L_i$ with $i = 1, 2, 3$]. j = for solving current iteratively.

TABLE 1. PMSG data.

PMSG	G_1	G_2	G_3
Outer diameter, mm	384	655	361
Axial length, mm	70	125	54
slots/poles	30/28	48/40	30/28
M_{active}	22.6	83.8	16.1
M_{PM}	2.6	7.0	0.96

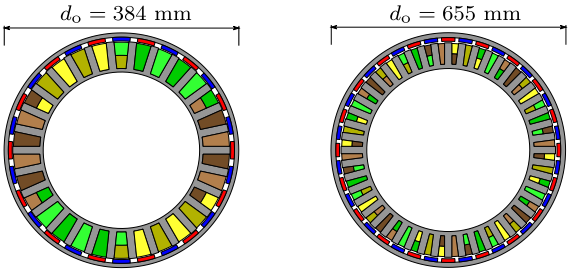

(a) G_1 (b) G_2 [22]

FIGURE 7. NO-PMSG cross sections (not to scale).

TABLE 2. Specified PMSG operating points for passive WECS case studies.

PMSG	G_1, G_3		G_2	
Operating point	n_c	n_r	n_c	n_r
Power, kW	0	4.2	0	12.5
Wind speed, m/s	3	12	3	10
Turbine speed, r/min	110	320	80	150
V_{bat}, V	48		240	

TABLE 3. Static FEA solution method results at rated operating point, n_r.

PMSG	G_1	G_2	G_3
P_g, kW	4.19	12.40	4.16
L_{ext}, mH	2.39	11.74	0.67
X_s, p.u.	0.48	0.39	1.47
X_{ext}, p.u.	1.71	0.94	0.47
X_{ext}/X_s	3.61	2.42	0.32
f_s, Hz	74.67	50.0	74.67
Turns per coil, N_s	13	19	22
V_{rms}	24.2	119.2	24.0
J, A/mm^2	5.1	6.3	6.5
δ	57.3°	51.6°	55.0°
η, %	92.8	93.0	90.0

To better illustrate the impedance matching results in Table 3, consider G_1's power curves in Fig. 8:

1) *Curve A* - This is G_1's power curve with zero external inductance added for impedance matching but with N_s adjusted for the specified cut-in speed at $n_c = 110$ r/min. The generated power increases steeply with turbine speed and shows poor generated power performance compared to the available wind turbine power.
2) *Curve B* - This is G_1's power curve with the necessary L_{ext} in Table 3 connected between the generator and the diode rectifier. The power curve shows that the generated power now almost exactly matches the available turbine power at the specified maximum power point n_r, and that with the calculated $L_{\text{ext}} = 2.39$ mH added to the passive WECS a substantial improvement in power matching is obtained.

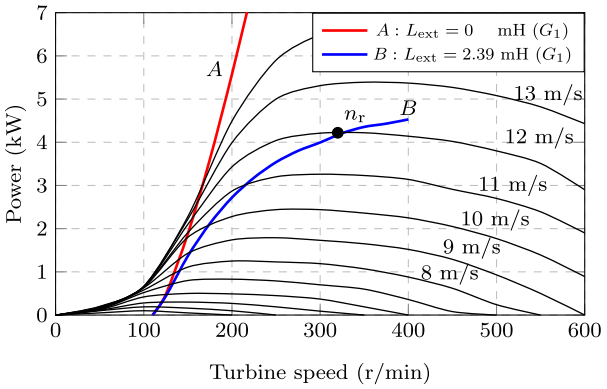

FIGURE 8. Power matching of G_1 with L_{ext} a parameter.

In Fig. 8 it is shown that, by adding L_{ext}, impedance matching can be used effectively as a method to improve power matching between the wind turbine and the wind generator in order to utilize more of the available wind power. The wind generator matches well with the turbine at low wind speeds, which is critical for the application, and still operates at the desired operating point at high wind speeds.

Incorporating external impedance matching into a site-specific design can also be done, similar to what is done in [6] for a specified wind cycle. In this case, the rated operating point, n_r, would then be determined using the specific site's annual wind profile. This will ensure that the wind generator achieves good power matching at low wind speeds and will increase annual energy harvesting.

B. 12.5 kW NO-PMSG Impedance Matching (G_2)

To investige the impedance matching of a 12.5 kW passive WECS, the NO-PMSG in [22] is used. The NO-PMSG cross-section is shown in Fig. 7(b) and was initially designed in [22] as a directly grid-connected 15 kW PM wind generator. The aim is to convert/recycle the existing machine for the 12.5 kW passive WECS.

The static FEA solution method is used to calculate the new N_s for the desired cut-in speed and also L_{ext} for maximum power point operation, as specified for G_2 in Table 2. The summarized results in Table 3 show that, with the calculated L_{ext} added to the 12.5 kW passive WECS, G_2 now matches with the rated generated power P_g at the specified operating point. The generator's power matching is shown in Fig. 9. Again, both operating power curves are given for the cases where $L_{\text{ext}} = 0$ mH and the calculated $L_{\text{ext}} = 11.74$ mH are added to the passive WECS.

Generator G_2's results show that by rewinding the existing machine and adding L_{ext}, as calculated with the static FEA solution method, impedance matching can be used effectively to "recycle" machines for small-scale passive WECSs. Moreover, by considering the results of both PMSGs G_1 and G_2, for small-scale passive WECSs it is shown that any generator can be matched with any wind turbine (provided that the generator's rated power is sufficient).

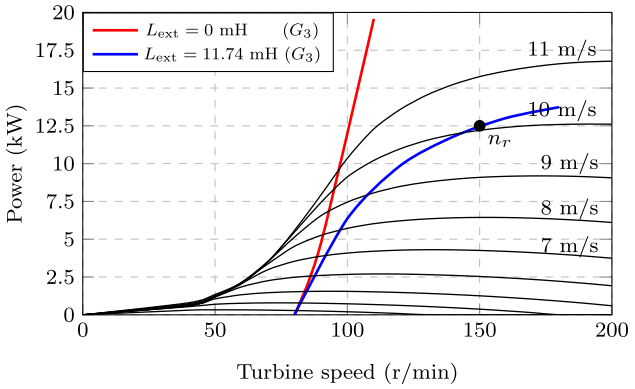

FIGURE 9. Power matching of G_3 with L_{ext} a parameter.

C. ADDITIONAL DISCUSSION

The above results indicate that external impedance matching in small-scale passive WECSs works excellently and is particularly suited for, but not limited to, rural stand-alone systems. The specifications in Table 2 and the power levels for the 4.2 kW and 12.5 kW case studies, were chosen according to what is considered realistic for this application. Theoretically there is no power limit for applying impedance matching in passive WECSs. However, at power levels higher than 20 kW, it is necessary to adapt the WECS's design from the simple fixed-pitch turbine and yaw-tail to a more sophisticated WECS with active pitch and yaw control that uses power converter machine drives. In these more sophisticated WECSs, active synchronous rectifiers or diode bridge rectifiers with dc-to-dc converters, such as the Enercon wind turbines [23], are then used to control the wind turbine generator.

Further considering the results for the proposed passive WECS presented in Fig. 8 and Fig. 9: It is evident that, by adding L_{ext} to the passive system, the power is limited independent of wind speed. Therefore, external impedance matching provides additional protection against generator demagnetization currents. Without external impedance matching ($L_{ext} = 0$ in Fig. 8 and Fig. 9) there is the risk of over-current damage and magnet demagnetization at extreme wind speeds.

VII. WIND GENERATOR DESIGN OPTIMIZATION

The static FEA method described in Section V can also be used when designing wind generators specifically for small-scale passive WECSs: Designing the wind generator for a desired performance whilst reducing the generator's total cost and mass is particularly of interest. However, the design process is significantly more complicated when still trying to achieve good power matching with the wind turbine at all wind speeds. Using external impedance matching with the proposed solution method can simplify the design process.

A. 4.2 kW NO-PMSG (G_3)

The proposed solution method is used together with an optimization algorithm to optimally design the NO-PMSG topology in Fig. 7(a) for the 4.2 kW passive WECS. Here, the NSGA-II optimization algorithm is used with a multi-objective function to create a pareto front of all the non-dominated design solutions. The aim of the multi-objective function is to minimize the active mass, M_{active}, and the permanent magnet mass, M_{PM}, of the NO-PMSG, whilst still adhering to the design constraints. The multi-objective function is given by

$$\min_{\mathbf{X}} \mathbf{F}(\mathbf{X}) = \min_{\mathbf{X}} \begin{bmatrix} M_{active}(\mathbf{X}) \\ M_{PM}(\mathbf{X}) \end{bmatrix}, \tag{26}$$

where $\mathbf{X}$ is the PMSG's dimensional array. For calculating M_{active}, all of the components shown in Fig. 7 are included, apart from the copper mass of the end-windings. The design constraints are chosen as

$$\mathbf{U} = \begin{bmatrix} P_g \\ \eta \\ J \end{bmatrix} = \begin{bmatrix} 4.2 \text{ kW} \\ \geq 90\% \\ \leq 6.5 \text{ A/mm}^2 \end{bmatrix}, \tag{27}$$

where J is the maximum allowed rated generator current density.

The design optimization process aims to achieve the multi-objective function in (26) by varying the dimensions of the NO-PMSG and uses the proposed static FEA method to calculate the performance and to ensure maximum power matching. In this way, the cost of the generator is effectively minimized for the correct L_{ext}.

B. RESULTS DISCUSSION

Generator G_3 in Table 1 and Table 3 is one of the pareto front solutions obtained from the multi-objective optimization. It is shown that the generator achieves maximum power matching at the rated operating point and that the performance constraints in (27) are met. Furthermore, M_{active} and M_{PM} are considerably reduced compared to generator G_1, showing that the proposed static FEA method can be used as an effective tool in the design optimization process.

VIII. CALCULATION METHOD: ANALYTICAL VS STATIC FEA

The analytically calculated L_{ext} using (10) and the calculated L_{ext} using the proposed static FEA solution method for generators $G_1 - G_3$'s power matching are compared in Table 4. It is shown in Table 4 that the analytically calculated L_{ext} is overestimated and that, as a result, the generated power P_g is less than the rated maximum power. This can be attributed to the lower analytically calculated L_s in Table 4. Also shown is the difference between L_d and L_q of the surface mounted PMSG due to saturation. Generator $G_1 - G_3$'s power curves, with the respective L_{ext} values from Table 4, are given in Fig. 10 to show the overall power matching errors. All this confirms the necessity of the proposed static FEA method for precise power matching calculation using iron-cored PMSGs.

It is also important that the static FEA method be computationally efficient, since it requires a total of 10 static FEA solutions. The static FEA solutions were performed on

TABLE 4. Analytical versus static FEA results.

PMSG	G_1		G_2		G_3	
	Anal.	FEA	Anal.	FEA	Anal.	FEA
P_g, kW	3.90	4.19	11.39	12.40	3.77	4.16
L_{ext}, mH	2.57	2.39	13.32	11.74	0.96	0.67
L_s, mH	0.67	0.81	4.44	5.49	2.05	2.48
L_q, mH	-	0.73	-	5.28	-	2.14
L_d, mH	-	0.58	-	4.43	-	2.04
L_e, mH	0.15	0.15	0.63	0.63	0.36	0.36

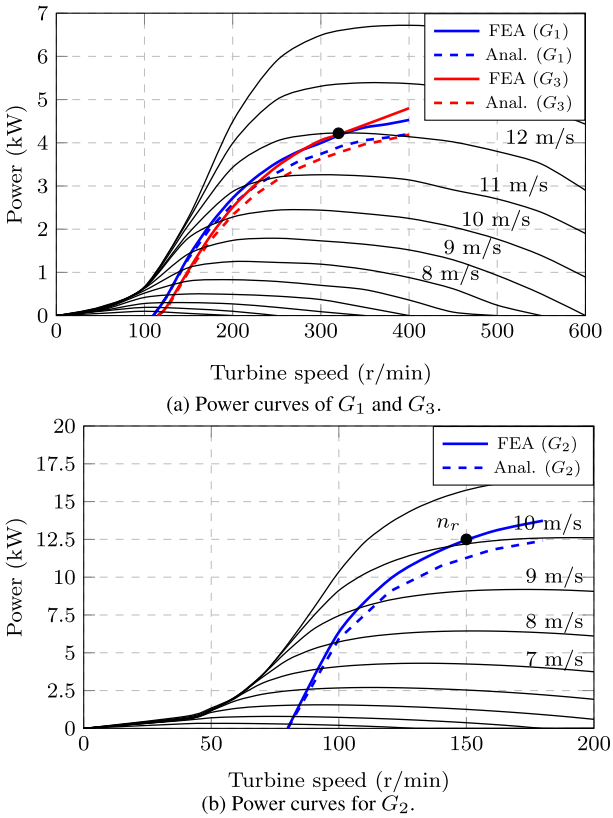

(a) Power curves of G_1 and G_3.

(b) Power curves for G_2.

FIGURE 10. Power matching curves comparing the analytical calculation and static FEA solution method, with the L_{ext} values from Table 4 a parameter.

a 3.20 GHz Intel(R) Core i7 CPU with 32 GB RAM. The computer solution time to complete the method in Fig. 6, for G_1, is on average 26 s; note that this is for full cross-section static FEA solutions of G_1 in Fig. 7(a).

IX. EXPERIMENTAL RESULTS

In this section, the accuracy of the proposed static FEA method for calculating L_{ext} and the improved power matching between the wind generator and wind turbine are verified through test results.

The test bench setup in Fig. 11 shows a manufactured NO-PMSG prototype that is connected via a torque sensor to a geared induction motor drive that emulates the wind turbine. The torque sensor is used to measure the input power. The NO-PMSG prototype has the same dimensions as G_1 in Table 3, only it was designed for a cut-in speed

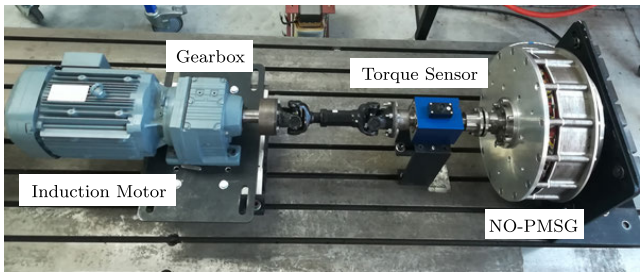

FIGURE 11. Experimental test bench setup of the manufactured NO-PMSG prototype.

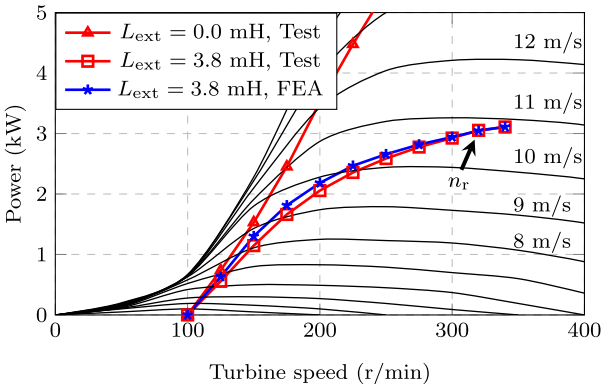

FIGURE 12. Measured and static FEA calculated power matching of the NO-PMSG prototype in the experimental passive system setup.

n_c = 100 rpm (N_s = 14) and has a lower copper fill factor due to the manufacturing of the preformed coils. To emulate the passive WECS in Fig. 2, the NO-PMSG's phase terminals are connected to a 48 V battery bank via an external inductance L_{ext}, a resistance R_c and a diode bridge rectifier. The available external inductance used in the tests is measured as L_{ext} = 3.8 mH.

Power measurements are taken at various turbine speeds with and without the external inductance connected between the NO-PMSG and the diode rectifier. The measured operating power curves are plotted in Fig. 12. The much improved power matching measured between the NO-PMSG and the wind turbine with L_{ext} = 3.8 mH is clearly shown in Fig. 12. The results prove that external impedance matching can be used effectively in passive WECSs to improve power matching. In practice, the battery terminal voltage is not constant and marginally increases due to the battery's state of charge. The equivalent modelling in Section III-A takes this accurately into account, with the measured battery terminal voltage varying between the predicted 48 V and 52 V.

To validate the equivalent modelling in Section IV and the static FEA solution results in Sections VI to VIII, the NO-PMSG prototype's generated power at the same turbine speed intervals are calculated using the static FEA solution method with L_{ext} = 3.8 mH. The static FEA calculated operating power curve is plotted in Fig. 12. The slight difference between the measured and predicted power curves at certain turbine speeds can be attributed to slight inaccuracies in the battery model, however, the difference is negligible. Further-

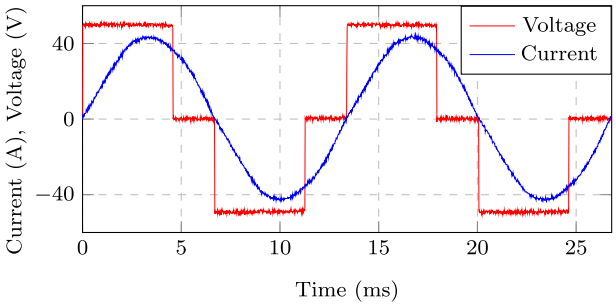

FIGURE 13. Measured current and line voltage waveforms at the diode bridge rectifier of the prototype passive generator system at 320 r/min and $L_{ext} = 3.8$ mH.

TABLE 5. Measured and the corresponding static FEA solution method results.

Parameter	Measured	Static FEA solution
n_r, r/min	320	320
L_{ext}, mH	3.8	3.77
P_g, kW	3.05	3.06

more, the measured voltage and current waveforms at the diode rectifier under rated operating conditions are shown in Fig. 13. It is shown that the generator current is close to sinusoidal and validates the proposed ac-equivalent system modelling where sinusoidal generator currents are assumed.

To validate the accuracy of the proposed solution method in Section V, that calculates the necessary L_{ext} for impedance matching, the following is done: The measured power value in Fig. 12 at a turbine speed of 320 r/min is taken as the NO-PMSG prototype operating point for which L_{ext} must be calculated. This operating point is at $n_r = 320$ r/min and $P_g = 3.05$ kW. Solving L_{ext} with the static FEA solution method yields $L_{ext} = 3.77$ mH and the generated power at $n_r = 320$ r/min is $P_g = 3.06$ kW. The results are summarized in Table 5. By comparison, the results in Table 5 are almost exact and validate the accuracy of the proposed static FEA solution method.

X. CONCLUSION

In this paper external impedance matching in small-scale passive WECSs is investigated for improved power matching. A fast and accurate calculation method is proposed for the necessary external inductance. From the results the following conclusions are drawn:

It is shown with 4.2 kW and 12.5 kW passive WECS case studies that the external impedance matching method can be used effectively to improve power matching between the wind generator and the wind turbine. Furthermore, this can be applied to any existing wind generator with a sufficient rated power and wind turbine.

The proposed method to calculate the required L_{ext} is shown to be accurate and computationally efficient. It is also shown that analytical methods to calculate L_{ext} can be inaccurate when iron-cored PMSGs are used and that the proposed method, using static FEA solutions, is necessary.

Including the proposed calculation method in the design optimization of the generator works excellently. The method can also be included in wind site-specific design optimization, maximizing annual wind energy harvesting and minimizing generator and external inductance sizes.

The accuracy of the proposed static FEA solution method and the improved power matching are confirmed by measured results.

APPENDIX A: ANALYTICAL INDUCTANCE CALCULATIONS

The magnetization inductance, L_m, is given by

$$L_m = \frac{m(Wk_{wj})^2 d_i l \mu_0}{\pi p^2 g'_{air} K_s}, \tag{28}$$

where m is the number of phases, W is the number of turns in series per phase, k_{wj} is the winding factor of the generator's working harmonic, d_i is the air gap diameter, l is the axial length, g'_{air} is the resultant air gap length taking Carter's factor into account [24] and K_s is the saturation factor.

The differential harmonic leakage flux coefficient, τ_d, is calculated from the harmonic analysis as in [25] and is given by

$$\tau_d = \frac{\sum_{n \neq j} (\frac{k_{wn}}{n})^2}{(\frac{k_{wj}}{j})^2}. \tag{29}$$

The slot-leakage inductance, L_{sl}, is calculated using

$$L_{sl} = \frac{4m}{Q_s} \mu_0 l W^2 \lambda_{uv} \tag{30}$$

as in [26]. Here, λ_{uv} is the slot permeance factor given in [26] for a double-layer non-overlapping winding with a vertical arrangement of coil sides, or as given in [21] for overlapping windings, and Q_s is the number of slots.

FIGURE 14. Wind turbine structure.

APPENDIX B: WIND TURBINE

The wind turbine structure, from which wind turbine data for the 4.2 kW case studies in this paper is obtained, is shown in Fig. 14. The wind turbine for the 12.5 kW case study has the same structure.

Regarding system protection: The blades and generator are off-centre in relation to the turbine tower. Under extreme conditions, the wind pushes the turbine and generator out of the wind with a mechanical yaw-mechanism that connects the nacelle to the tower, which lowers the input power from the turbine.

Because the horizontal axis wind turbine has a full degree of rotation, brush-slip-rings are necessary in the nacelle for power transmission. Note that the impedance matching for passive WECSs presented in this paper is not limited to this type of wind turbine technology.

REFERENCES

[1] S. Li, T. A. Haskew, and L. Xu, "Conventional and novel control designs for direct driven PMSG wind turbines," *Electr. Power Syst. Res.*, vol. 80, no. 3, pp. 328–338, Mar. 2010.
[2] M. A. Abdullah, A. H. M. Yatim, C. W. Tan, and R. Saidur, "A review of maximum power point tracking algorithms for wind energy systems," *Renew. Sustain. Energy Rev.*, vol. 16, no. 5, pp. 3220–3227, Jun. 2012.
[3] R. Kot, M. Rolak, and M. Malinowski, "Comparison of maximum peak power tracking algorithms for a small wind turbine," *Math. Comput. Simul.*, vol. 91, pp. 29–40, May 2013.
[4] M. Arifujjaman, M. T. Iqbal, and J. E. Quaicoe, "Reliability analysis of grid connected small wind turbine power electronics," *Appl. Energy*, vol. 86, no. 9, pp. 1617–1623, Sep. 2009.
[5] J. A. Stegmann and M. J. Kamper, "Economic and efficiency evaluation of different battery charging wind generator systems," in *Proc. Southern Afr. Universities Power Eng. Conf. (SAUPEC)*, Johannesburg, South Africa, 2010, pp. 205–210.
[6] B. Sareni, A. Abdelli, X. Roboam, and D. H. Tran, "Model simplification and optimization of a passive wind turbine generator," *Renew. Energy*, vol. 34, no. 12, pp. 2640–2650, Dec. 2009.
[7] Z. Alnasir and M. Kazerani, "An analytical literature review of stand-alone wind energy conversion systems from generator viewpoint," *Renew. Sustain. Energy Rev.*, vol. 28, pp. 597–615, Dec. 2013.
[8] W. Liang and W. Liu, "Key technologies analysis of small scale non-grid-connected wind turbines: A review," in *Proc. World Non-Grid-Connected Wind Power Energy Conf.*, Nov. 2010, pp. 1–6.
[9] J. G. Aredjodoun, P. K. Chetangny, S. Houndedako, A. Vianou, D. Chamagne, and C. Espanet, "Optimal adaptation of the wind rotor to the permanent magnets synchronous generator of a small passive wind turbine," in *Proc. IEEE PES/IAS PowerAfrica*, Aug. 2019, pp. 164–169.
[10] D.-H. Tran, B. Sareni, X. Roboam, and C. Espanet, "Integrated optimal design of a passive wind turbine system: An experimental validation," *IEEE Trans. Sustain. Energy*, vol. 1, no. 1, pp. 48–56, Apr. 2010.
[11] D. H. Tran, B. Sareni, X. Roboam, E. Bru, and A. De Andrade, "Robust design of a passive wind turbine system," *COMPEL, Int. Comput. Math. Elect. Electron. Eng.*, vol. 31, no. 3, pp. 932–944, 2012.
[12] S. O. Ani, H. Polinder, and J. A. Ferreira, "Comparison of energy yield of small wind turbines in low wind speed areas," *IEEE Trans. Sustain. Energy*, vol. 4, no. 1, pp. 42–49, Jan. 2013.
[13] F. G. Rossouw and M. J. Kamper, "Use of air-cored axial flux permanent magnet generator in direct battery charging wind energy systems," in *Proc. 7th Int. Conf. Power Electron. Drive Syst.*, Nov. 2007, pp. 1102–1107.
[14] C. J. J. Labuschagne and M. J. Kamper, "Performance analysis of direct-drive PM synchronous wind generator for maximum power point direct battery charging," in *Proc. 13th Int. Conf. Electr. Mach. (ICEM)*, Sep. 2018, pp. 358–364.
[15] S. O. Ani, H. Polinder, and J. A. Ferreira, "Small wind power generation using automotive alternator," *Renew. Energy*, vol. 66, pp. 185–195, Jun. 2014.
[16] J. S. Artal-Sevil, R. Dufo, J. A. Dominguez, and J. L. Bernal-Agustín, "Small wind turbines in smart grids. Transformation of electrical machines in permanent magnet synchronous generators," in *Proc. 13th Int. Conf. Ecol. Vehicles Renew. Energies (EVER)*, Apr. 2018, pp. 1–8.
[17] N. Mohan, T. M. Undeland, and W. P. Robbins, *Power Electronics: Converters, Applications, and Design*. Hoboken, NJ, USA: Wiley, 2003.
[18] M. J. Kamper, C. Africa, C. J. J. Labuschagne, and L. P. Mdakane, "Line reactance criteria for minimizing line current harmonic content in diode rectifier connected wind generator systems," in *Proc. Southern Afr. Universities Power Eng. Conf. (SAUPEC)*, Cape Town, South Africa, Jan. 2020, pp. 1–6.
[19] Y. Xia, K. H. Ahmed, and B. W. Williams, "Different torque ripple reduction methods for wind energy conversion systems using diode rectifier and boost converter," in *Proc. IEEE Int. Electr. Mach. Drives Conf. (IEMDC)*, May 2011, pp. 729–734.
[20] J. H. J. Potgieter and M. J. Kamper, "Calculation methods and effects of end-winding inductance and permanent-magnet end flux on performance prediction of nonoverlap winding permanent-magnet machines," *IEEE Trans. Ind. Appl.*, vol. 50, no. 4, pp. 2458–2466, Jul. 2014.
[21] J. Pyrhonen, T. Jokinen, and V. Hrabovcova, *Design of Rotating Electrical Machines*. Hoboken, NJ, USA: Wiley, 2013.
[22] J. H. J. Potgieter and M. J. Kamper, "Design optimization of directly grid-connected PM machines for wind energy applications," *IEEE Trans. Ind. Appl.*, vol. 51, no. 4, pp. 2949–2958, Jul. 2015.
[23] M. Ragheb, "Modern wind generators," Univ. Illinois Urbana-Champaign, Champaign, IL, USA, Tech. Rep., Feb. 2019. [Online]. Available: https://mragheb.com/NPRE%20475%20Wind%20Power%20Systems/Modern%20Wind%20Generators.pdf
[24] B. Heller and V. Hamata, *Harmonic Field Effects in Induction Machines*. Amsterdam, The Netherlands: Elsevier, 1977.
[25] A. J. Rix, "Design, comparison and experimental evaluation of non-overlap winding radial flux permanent magnet hub drives for electric vehicles," Ph.D. dissertation, Dept. Elect. Electron. Eng., Univ. Stellenbosch, Stellenbosch, South Africa, 2011.
[26] C. Madariaga, W. Jara, J. A. Tapia, J. Pyrhonen, P. Lindh, and J. A. Riedemann, "Closed-form solution for the slot leakage inductance of tooth-coil-winding permanent magnet machines," *IEEE Trans. Energy Convers.*, vol. 34, no. 3, pp. 1572–1580, Sep. 2019.

CASPER J. J. LABUSCHAGNE (Student Member, IEEE) studied electrical and electronic engineering at Stellenbosch University, Stellenbosch, South Africa, where he is currently pursuing the Ph.D. degree in electrical engineering.

MAARTEN J. KAMPER (Senior Member, IEEE) received the M.Sc. (Eng.) and Ph.D. (Eng.) degrees from Stellenbosch University, Stellenbosch, South Africa, in 1987 and 1996, respectively. He has been with the Academic Staff of the Department of Electrical and Electronic Engineering, Stellenbosch University, since 1989. He is currently a Distinguished Professor of electrical machines and drives. His research interests include computer-aided design and control of reluctance, permanent-magnet, and induction machine drives. He is also a South African National Research Foundation-Rated Researcher. He is also a Registered Professional Engineer in South Africa.